WATER RESOURCES RESEARCH, VOL. 26, NO. 8, PAGES 1819–1832, AUGUST 1990

Similarity and Length Scale for Spatially Varied Overland Flow

PIERRE Y. JULIEN AND GLENN E. MOGLEN

Department of Civil Engineering, Colorado State University, Fort Collins

One-dimensional finite element models enable physically based investigations of overland flow generated under spatially varied surface slope, width, roughness, and excess rainfall intensity. Simulated results of 8400 dimensionless hydrographs under spatially varied input parameters indicate that runoff discharge variations depend primarily on the ratio of rainfall duration t_r to the time to equilibrium t_e. Peak discharge distributions change drastically as the dimensionless rainfall duration t_r/t_e approaches unity. Similarity conditions exist for all four parameters regardless of whether the spatial variability is correlated or uncorrelated. A length scale function of not only the spatially averaged values of surface parameters but also depending on rainstorm duration and intensity delineates similarity conditions for spatially varied surface runoff. For surface runoff lengths much shorter than this length scale, the rainfall-runoff relationship becomes nearly independent of the spatial variability in hydrologic parameters. Conversely, for surface runoff lengths exceeding the length scale, the rainfall-runoff relationship is sensitive to spatial variability. This length scale can serve as a basis for the determination of grid sizes in hydrologic models.

INTRODUCTION

The influence of the spatial variability of rainfall precipitation, infiltration, surface roughness and surface topography on surface runoff characteristics has been widely recognized in hydrology. Rainfall precipitation has received considerable attention in the recent literature, *Amorocho and Wu* [1977] simulated spatially distributed precipitation fields using a randomization process to generate clusters of short-lived and high intensity rain cells within a storm band. *Gupta and Waymire* [1979] investigated the stochastic structure of space-time rainfall fields. *Woolhiser and Osborn* [1985] examined the temporal features of accumulated point rainfall precipitation in dimensionless form while *Valdes et al.* [1985] considered three one-dimensional models of point rainfall precipitation. More recently, *Rodriguez-Iturbe and Eagleson* [1987] demonstrated the feasibility of modeling the spatial and temporal structure of rainfall events through mathematical multidimensional point process techniques.

The spatial variability of infiltration characteristics has also been examined by *Smith and Hebbert* [1979], in which Monte Carlo simulations of the random distribution of soil properties lead to the conclusion that gradual S-shaped infiltration curves result from randomly nonuniform soil surfaces. *Maller and Sharma* [1981] extended previous investigations in light of Philip's infiltration equation. *Sivapalan and Wood* [1986] derived quasi-analytical expressions for the ponding time and infiltration rate under two conditions: (1) spatially variable soils and uniform rainfall, and (2) constant soil properties and spatially variable rainfall. They concluded that rainfall is expected to play a more critical role in rainfall-runoff modeling since the correlation length of rainfall is usually larger than that of soil hydraulic conductivity. It has also been suggested that biased mean areal infiltration responses result from spatially variable soil and rainfall when average soil properties and rainfall intensity are used. Comprehensive treatments of runoff prediction errors and bias in parameter estimation induced by spatially varied precipitation together with a Green-Ampt infiltration equation have been pursued by *Troutman* [1983, 1985*a*, *b*].

Routing surface runoff exhibits several intricacies. For instance, *Wilson et al.* [1979] stated that nobody will dispute the effect of spatial distribution of rainfall on the amount of surface runoff. They also pointed out that their experiments do not support the argument made in the past that errors in the rainfall input will be dampened when routed through a basin. They concluded that not only the spatial distribution of rainfall has a marked influence on the behavior of the runoff hydrograph from a small catchment, but the application of rainfall-runoff models without an appropriate description of the spatial character of the input may lead to unacceptable errors. If linear models for the simulation of rainfall-runoff relationships are widely used in regard of their simplified mathematical structure, it remains that surface runoff routing is highly nonlinear as recognized by *Diaz-Granados et al.* [1986]. It has long been known that the response time of a basin tends to decrease as storm intensity increases. *Dawdy* [1982] states that kinematic wave models constitute one step away from the linear storage assumption toward the use of a dynamic routing equation. He added that the kinematic wave equation tends to overcome the shortcoming that linear techniques, such as instantaneous unit hydrographs, are not identical for small and large storms. Major advantages of kinematic wave models are that parameters relate to the physical world, and these models are perfectly suited for use in distributed parameter models. He explains the disadvantage of distributed models in that they require more data and much more computer time to run when compared with lumped-parameter models. As computers get larger, faster and cheaper, however, this disadvantage decreases in importance. He finally concluded that the trend in rainfall-runoff modeling is toward physically based distributed-parameter models.

Spatially varied overland flow has been investigated extensively by a number of researchers using both physical and analytical models. *Kibler and Woolhiser* [1970] used a kinematic cascade of planes and a converging conical surface to examine the effects of varying slope and width on computed discharge. *Machado and O'Donnell* [1977] analyzed the influence of spatial and temporal variability of model param-

Paper number 90WR00499.
0043-1397/90/90WR-00499$05.00

eters and rainfall input with given probability distributions on overland flow treated as a stochastic variable. Their analysis permits calculations of the variance of the outflow in terms of the sampling variance of the parameters. *Wu et al.* [1978] used a physical model to examine several different spatial distributions of roughness elements in an effort to develop criteria for the valid use of lumped parameters.

Self-similarity and scale problems have more recently been looked into. The investigation of *Sharma et al.* [1983] implies the definition of a zone of influence, or a spatial scale beyond which the spatial correlation for a given property could be neglected. *Milly and Eagleson* [1987] inferred that the problem of spatial integration to the catchment scale is not trivial because the analysis of small-scale physical processes in catchments suggest that the local response is a nonlinear function of these variables. They examined the extent to which the spatial variability of soil and vegetation affect the temporal-spatial averages of the major hydrologic fluxes. They sought the existence of an equivalent homogeneous soil capable of reproducing the average behavior of an inhomogeneous area. *Caroni et al.* [1986] dealt with the problem of detecting nonlinearity and time-variance at the basin scale. The analysis has been performed where spatial variability of rainfall patterns, soil properties and vegetation cover would not appreciably affect the rainfall-runoff process. The integrating effects of variability should not dominate at such a drainage basin scale. *Sivapalan et al.* [1987] described a simple conceptual model of runoff production based on catchment topography and the spatial variability of rainfall and soil properties. They formulated five similarity parameters and three dimensionless variables representing initial conditions and storm characteristics. *Wood et al.* [1988] reported results of a preliminary investigation into the existence of a representative elementary area (REA). They believe that at a small scale, actual patterns of topography, soil and rainfall characteristics are important in governing runoff production. Differences in actual patterns of variability between areas at this scale will produce different responses. However, as scale increases, all areas will yield almost identical responses for the case of stationary distributions. They consider that the hydrologic variables at every location within each catchment are related to its average value through some probability distribution. Each mathematical point in the continuum is associated with the area over which the average values are taken. The REA is defined as the averaging area acting as the smallest discernible point which is representative of the continuum. They concluded that the REA is strongly influenced by the topography.

As mentioned by *Amorocho* [1982], the simulation of spatially varied precipitation fields should not be considered as a necessary prescription for all catchments and all applications. Depending on the catchment response to storm field variabilities, these simulations may not be justified from practical and economical standpoints; to omit the simulations in other cases may lead to gross inaccuracies in hydrological applications. We concur with his conclusion that research on objective methods to make this determination is urgently needed. Not only is research needed for spatially varied precipitation fields, but it should be extended to the analysis of topography, infiltration and excess rainfall, vegetation and surface roughness.

The specific objective of this study is to quantify the influence of spatial variability in slope, surface roughness, surface width, and excess rainfall intensity on surface runoff characteristics. Reference systems are modeled with spatially averaged values of the hydrologic parameters. The differences between computed surface runoff hydrographs for reference systems versus spatially varied systems are examined in dimensionless form for complete and partial equilibrium hydrographs. The analysis of the rainfall-runoff response under spatially varied hydrologic conditions serves to define a length scale describing similar surface runoff conditions.

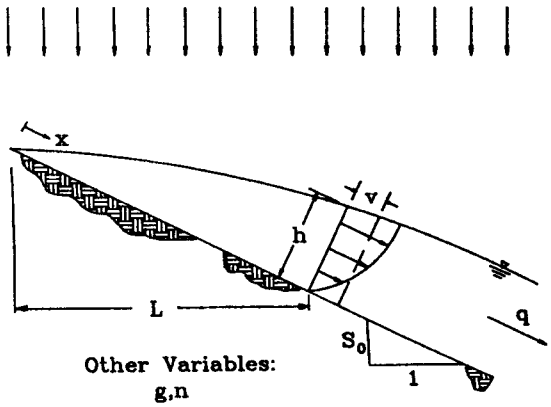

Fig. 1. Overland flow parameters.

The methodology proposed for this analysis of spatially varied conditions differs from the above cited studies. Numerical models are called for because analytical solutions to spatially varied nonlinear systems cannot be derived even for the most simple case. The selected one-dimensional finite element model solves the kinematic wave approximation of the St-Venant equations. The results are expressed in dimensionless form after considering that the time to equilibrium serves as an important physical characteristic. Similarities are preserved by keeping the same spatially averaged input parameters for each system. Also, the same excess rainfall volume is maintained in each system in order to avoid the error and bias problems discussed in the recent literature.

Fundamentals of Overland Flow

The overland flow system shown in Figure 1 illustrates the following overland flow parameters: L is the length of the horizontal projection of the overland flow plane, h is the flow depth, v is the average flow velocity, S_0 is the average slope gradient, i is the excess rainfall intensity, and q is the discharge per unit width. Note that excess rainfall intensity obtained by subtracting the rate of infiltration from rainfall intensity is considered in the analysis. Infiltration combines both the conventional Hortonian infiltration excess mechanism with Dunne's saturation excess runoff production mechanism. In the following the interaction between surface and subsurface flow is not being separately considered but treated as excess rainfall intensity. Four additional parameters are the plane width w, the gravitational acceleration g, the Manning roughness coefficient n, and the total discharge $Q = wq$.

The governing equations for overland flow are the St-Venant momentum and continuity equations. Derivations of these equations may be found in the works by *Henderson and Wooding* [1964], *Woolhiser and Liggett* [1967], *Eagle-*

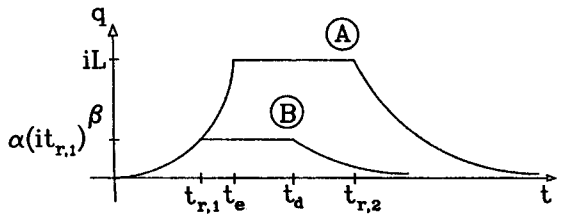

Fig. 2. Complete and partial equilibrium hydrographs.

son [1970] and *Overton and Meadows* [1976]. The St-Venant equations which account for unsteady nonuniform flow may be simplified to the kinematic wave approximation which is applicable under most overland flow conditions.

Conservation of mass for one-dimensional overland flow with variable surface width yields the following form of the continuity equation:

$$w\frac{\partial h}{\partial t}+\frac{\partial Q}{\partial x}-wi=0 \tag{1}$$

Notice that under spatially varied width, a two-dimensional system is actually considered.

Resistance to flow is expressed in terms of a stage-discharge relationship:

$$Q=\alpha h^{\beta} \tag{2}$$

Several resistance equations describe the various types of overland flow conditions depending on whether the flow is laminar or turbulent, and whether the boundary is smooth or rough. These conditions have been examined by *Julien and Simons* [1985], and the Manning resistance equation has been arbitrarily selected for the purpose of this study. Preliminary investigations by *Julien et al.* [1988] and *Moglen* [1989] showed comparable results with other resistance equations. After combining the Manning resistance equation with the kinematic wave approximation, the following expressions for α and β are obtained:

$$\alpha=\frac{S_0^{1/2}w}{n} \tag{3}$$

$$\beta=\frac{5}{3} \tag{4}$$

It can be noted that the kinematic wave approximation requires that slopes cannot be negative or zero.

An important physical characteristic of overland flow planes with constant slope, width, roughness and rainfall intensity is the time to equilibrium t_e given by the relationship:

$$t_e=\left(\frac{wL}{\alpha i^{\beta-1}}\right)^{1/\beta} \tag{5}$$

As shown in Figure 2, a complete equilibrium hydrograph (hydrograph A), is obtained when the rainfall duration $t_{r,2}$ exceeds the time to equilibrium t_e. For rainfall durations $t_{r,1}$ shorter than the time to equilibrium t_e the resulting partial equilibrium hydrograph is sketched as hydrograph B.

In terms of the linearity of the rainfall-runoff response, the hydrographs in Figure 2 indicate that partial equilibrium hydrographs are nonlinear because the magnitude of the peak discharge depends on both the duration and intensity of rainfall. Similarly, the duration of peak discharge for partial equilibrium hydrographs $t_d - t_{r,1}$ also depends on a complex function of rainfall duration and intensity. On the other hand, as the rainfall duration t_r becomes much larger than the time to equilibrium t_e, the response of complete hydrographs becomes asymptotically linear, because the magnitude of peak discharge increases linearly with rainfall intensity. Also, the duration of complete equilibrium peak discharge $t_r - t_e$ becomes asymptotically equal to rainfall duration t_r when $t_r \gg t_e$.

In the following analysis, excess rainfall intensity is allowed to vary in space but not in time. The additional effects of spatial variability in slope, width, and surface roughness are accounted for after substituting (2) into (1):

$$w\frac{\partial h}{\partial t}+\alpha\beta h^{\beta-1}\frac{\partial h}{\partial x}+h^{\beta}\frac{\partial \alpha}{\partial x}-wi=0 \tag{6}$$

where the second and third terms from the left account for the spatial variation in discharge. From (6) and (3) the spatial variability of both slope S_0 and surface roughness n is reflected in the second and third terms of (6). On the other hand, the spatial variability of excess rainfall intensity i is accounted for in the last term of (6), while surface width w is included in all terms of (6). Equation (6) is solved for flow depth as a function of space and time, then converted into runoff discharge from (2).

Finite Element Formulation

Numerical modeling of overland flow has evolved considerably as digital computers have become faster and more common. Originally, the method of characteristics was used to find "the space-time locus of discontinuity in the partial derivatives" [*Eagleson*, 1970]. In recent years, finite difference and finite element schemes have been used to solve the equations of motion for overland flow. These techniques are very flexible, allowing for a wider range of conditions while avoiding problems incurred by kinematic shocks as described by *Lighthill and Whitham* [1955]. A finite element scheme has been arbitrarily preferred for the following analysis. It is acknowledged that similar conclusions should be obtained from equivalent finite difference schemes. The comparison between finite difference and finite element schemes is, however, beyond the scope of this paper.

The one-dimensional finite element model CASC, briefly described here, provides numerical solutions to (6) from the Galerkin weighted residual method:

$$\int_L(\delta h)\frac{\partial h}{\partial t}w\,dx+\int_L(\delta h)\alpha\beta h^{\beta-1}\frac{\partial h}{\partial x}\,dx+\int_L(\delta h)h^{\beta}\frac{\partial \alpha}{\partial x}\,dx-\int_L(\delta h)wi\,dx=0 \tag{7}$$

where δh is a small variation from the flow depth h. Making use of the Jacobian determinant $|J|$, the shape function N, and the derivative of the shape function $\partial N/\partial\xi$ with respect to the local coordinate ξ, the following discretized form of (7) is obtained:

$$\int_L \langle \delta \mathbf{h} \rangle \{\mathbf{N}\}\langle \mathbf{N}\rangle \left\{ \mathbf{w} \frac{\Delta \mathbf{h}}{\Delta \mathbf{t}} \right\} |J|\, d\xi + \int_L \langle \delta \mathbf{h} \rangle \{\mathbf{N}\}\langle \mathbf{N}\rangle \{\alpha\beta \mathbf{h}^{\beta-1}\} \left\langle \frac{\partial \mathbf{N}}{\partial \xi} \right\rangle \{\mathbf{h}\}\, d\xi + \int_L \langle \delta \mathbf{h} \rangle \{\mathbf{N}\}\langle \mathbf{N}\rangle \{\mathbf{h}^{\beta}\} \left\langle \frac{\partial \mathbf{N}}{\partial \xi} \right\rangle \{\alpha\}\, d\xi - \int_L \langle \delta \mathbf{h} \rangle \{\mathbf{N}\}\langle \mathbf{N}\rangle \{\mathbf{wi}\} |J|\, d\xi = 0 \quad (8)$$

Note that braces indicate a column vector, while angle brackets indicate a row vector. Using Gaussian quadrature for each element, (8) is integrated and assembled into two global matrices $[C]$ and $[K]$, and one vector $\{\mathbf{F}\}$:

$$[C] = \{\mathbf{N}\}[\langle \mathbf{N}\rangle \{\mathbf{w}\}]\langle \mathbf{N}\rangle |J| \quad (9)$$

$$[K] = \{\mathbf{N}\}\left[\langle \mathbf{N}\rangle \{\mathbf{h}^{\beta-1}\} \left(\left\langle \frac{\partial \mathbf{N}}{\partial \xi} \right\rangle \{\alpha\} \langle \mathbf{N}\rangle + \langle \mathbf{N}\rangle \{\alpha\beta\} \left\langle \frac{\partial \mathbf{N}}{\partial \xi} \right\rangle \right) \right] \quad (10)$$

$$\{\mathbf{F}\} = \{\mathbf{N}\}\langle \mathbf{N}\rangle \{\mathbf{wi}\} |J| \quad (11)$$

The resulting matrix formulation is

$$[C]\left\{ \frac{\Delta \mathbf{h}}{\Delta \mathbf{t}} \right\} + [K]\{\mathbf{h}\} - \{\mathbf{F}\} = 0 \quad (12)$$

The initial boundary condition imposes no flow depth at all nodes for the first time step, and the upstream boundary is held fixed at zero flow depth at subsequent time steps. The following implicit numerical scheme [*Dhatt and Touzot*, 1984] is solved iteratively:

$$\{\Delta \mathbf{h}^j_{t+\Delta t}\} = ([C] + \Delta t[K])^{-1}((\{\mathbf{F}\} - [K]\{\mathbf{h}^j_{t+\Delta t}\})\Delta t + [C](\{\mathbf{h}_t\} - \{\mathbf{h}^j_{t+\Delta t}\})) \quad (13)$$

where the depth vector $\{\mathbf{h}\}$ is incremented by an amount $\{\Delta \mathbf{h}\}$ using

$$\{\mathbf{h}^1_{t+\Delta t}\} = \{\mathbf{h}_t\} \qquad j = 0 \quad (14)$$

$$\{\mathbf{h}^{j+1}_{t+\Delta t}\} = \{\mathbf{h}^j_{t+\Delta t}\} + \{\Delta \mathbf{h}^j_{t+\Delta t}\} \qquad j > 0 \quad (15)$$

Calculations at iteration j are performed between (13) and (15) until the vector $\{\Delta \mathbf{h}\}$ becomes negligible.

This algorithm enables the simulation of stationary storms (this paper) or moving storms [*Richardson*, 1989]. The interested reader is referred to *Julien et al.* [1988] for more details regarding the mathematical formulation, code description, simulation examples for stationary and moving rainstorms, and comparison with observed data.

In the following sections, two sets of conditions are considered for the spatially varied analysis in slope, width, surface roughness and excess rainfall precipitation: (1) in the next section, each parameter is examined separately under spatially uncorrelated random fields; and (2) the effects of spatially varied slope are then examined separately under correlated conditions given from field spectral density data.

Uncorrelated Spatial Variability

The effects of each parameter variation on the discharge hydrograph are investigated separately for uncorrelated spatially varied slope, Manning n, width, and excess rainfall intensity. The terminology "uncorrelated" spatial variability refers to the selection of nodal parameter values which are independent of the values at adjacent nodes. The use of excess rainfall intensity instead of rainfall intensity accommodates the following two situations: (1) spatially varied rainfall precipitation and constant infiltration; and (2) constant rainfall precipitation and spatially varied infiltration. Infiltration here refers to both the Hortonian infiltration mechanism with Dunne's saturation excess runoff production mechanism treated jointly as excess rainfall. One may appropriately notice that the model CASC cannot simulate negative values of excess rainfall intensity. Dimensionless hydrographs are obtained from dimensionless discharge q/iL and dimensionless time t/t_e. The dimensionless rainfall duration t_r/t_e defines the ratio of rainfall duration t_r to the time to equilibrium t_e. When this parameter is less than 1, the hydrograph is said to reach partial equilibrium. Complete equilibrium hydrographs corresponds to $t_r/t_e > 1$.

Similar systems are simulated with identical time steps, number of nodes, and probability density functions of the spatially varied parameter. Preliminary investigations by *Julien et al.* [1988] and *Moglen* [1989] showed that (1) a constant time step equal to one-fourth of the time to equilibrium t_e is more than adequate to define a discharge hydrograph; (2) runoff discharge is relatively unaffected by the number of nodes, provided there is a minimum of seven nodes; and (3) the results of the forthcoming analysis are not sensitive to the probability density function selected for the variability of each parameter. Accordingly, the model CASC is applied with a spatial resolution of 11 equidistant nodes and a time resolution equal to one-tenth of the time to equilibrium.

Spatial perturbations are introduced when the nodal values X'_l of one of the four spatially varied parameters are randomly selected based on a uniform distribution around the reference value μ_x. The magnitude of the spatial variability of each parameter is defined by the perturbation scaling factor ϕ which describes the maximum allowable nodal value X'_l from

$$\mu_x\left(1 - \frac{\phi - 1}{\phi + 1}\right) \le X'_l \le \mu_x\left(1 + \frac{\phi - 1}{\phi + 1}\right) \quad (16)$$

The perturbation scaling factor ϕ controls the magnitude of the spatial variability. From (16) the transformation imposes that all values of plane width, surface slope, Manning n, and rainfall intensity are nonzero and positive, computer simulations being impossible otherwise. Notice that the quantity $(\phi - 1)/(\phi + 1)$ reduces to zero when $\phi = 1$, which defines a nonperturbed system. For very large ϕ values the same ratio approaches unity and the maximum variation from the mean is therefore $2\mu_x$. For systems discretized with 11 nodes the spatially averaged values of each parameter X are set equal to their respective constant reference value μ_x from the following modification of the previously assigned values of X'_l:

$$X_l = \left(\frac{11\mu_x}{X_1 + X_2 + X_3 + \cdots + X_{11}} \right) X'_l \quad (17)$$

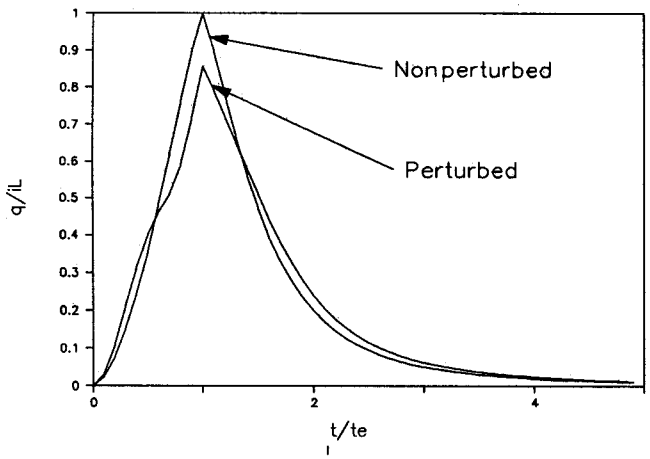

Fig. 3. Spatially varied and nonperturbed overland flow hydrographs.

Consequently, the spatially averaged properties of each parameter are preserved in order to compare systems which are strictly equivalent in terms of average properties, but variable only in terms of spatial distribution.

Consider the simulation of a single perturbed system as shown in Figure 3. While the nonperturbed system produces smooth rising and falling limbs, the spatially varied system creates fluctuations in discharge about the nonperturbed hydrograph.

Several sets of 100 perturbed systems are generated. Identical volumes of water are routed through each of the 100 systems in order to provide comparisons of similar systems. The input parameter envelopes describe the maximum and minimum of those 100 parameter perturbations at each node. They are nondimensionalized after dividing by the reference value. Thus x^*, z^*, n^*, w^*, and i^*, respectively, denote dimensionless space, elevation, Manning coefficient, surface width, and excess rainfall intensity. Figures 4*a*–4*d* show the input parameter envelopes as a function of dimensionless space from upstream $x^* = 0$ to downstream $x^* = 1$. For instance, when $\phi = 2$, the highest and lowest value of the perturbed parameter at each node defines the input parameter envelope denoted with $\phi = 2H$ for the highest and $\phi = 2L$ for the lowest values. Similarly, the lines $\phi = 4H$ and $\phi = 4L$ define the input parameter envelopes when $\phi = 4$. These figures illustrate the effects of the parameter ϕ; envelopes are small when $\phi = 2$ and large when $\phi = 6$.

In order to investigate all possible permutations of the single parameter variability, it is important to recognize that there are three types of input parameters: (1) the duration of rainfall (partial or complete equilibrium), (2) the magnitude of parameter perturbation ϕ, and (3) the overland flow parameter to be varied (slope, Manning n, surface width, and excess rainfall intensity). Three different rainfall durations covering the range from partial to complete equilibrium

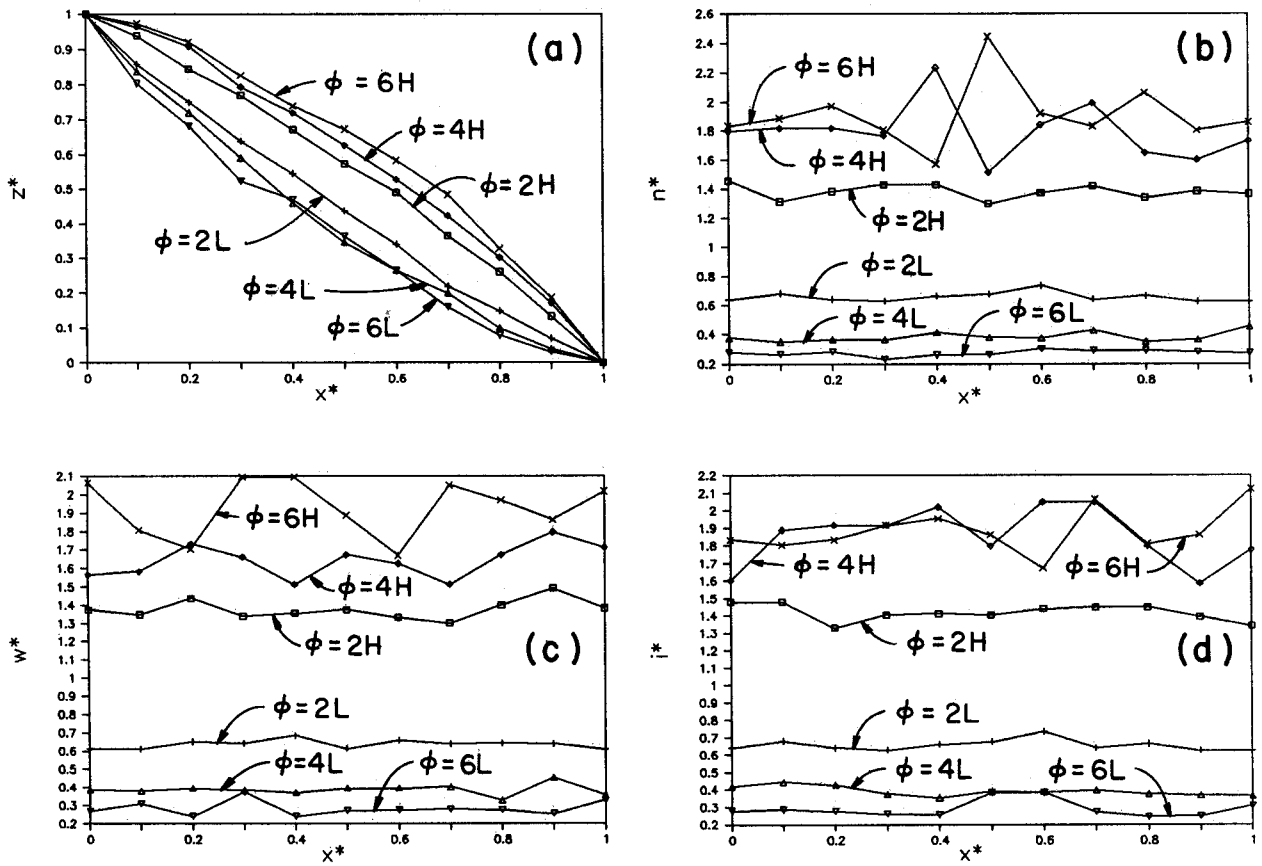

Fig. 4. Input Envelopes for (*a*) slope, (*b*) Manning n, (*c*) surface width, and (*d*) rainfall intensity.

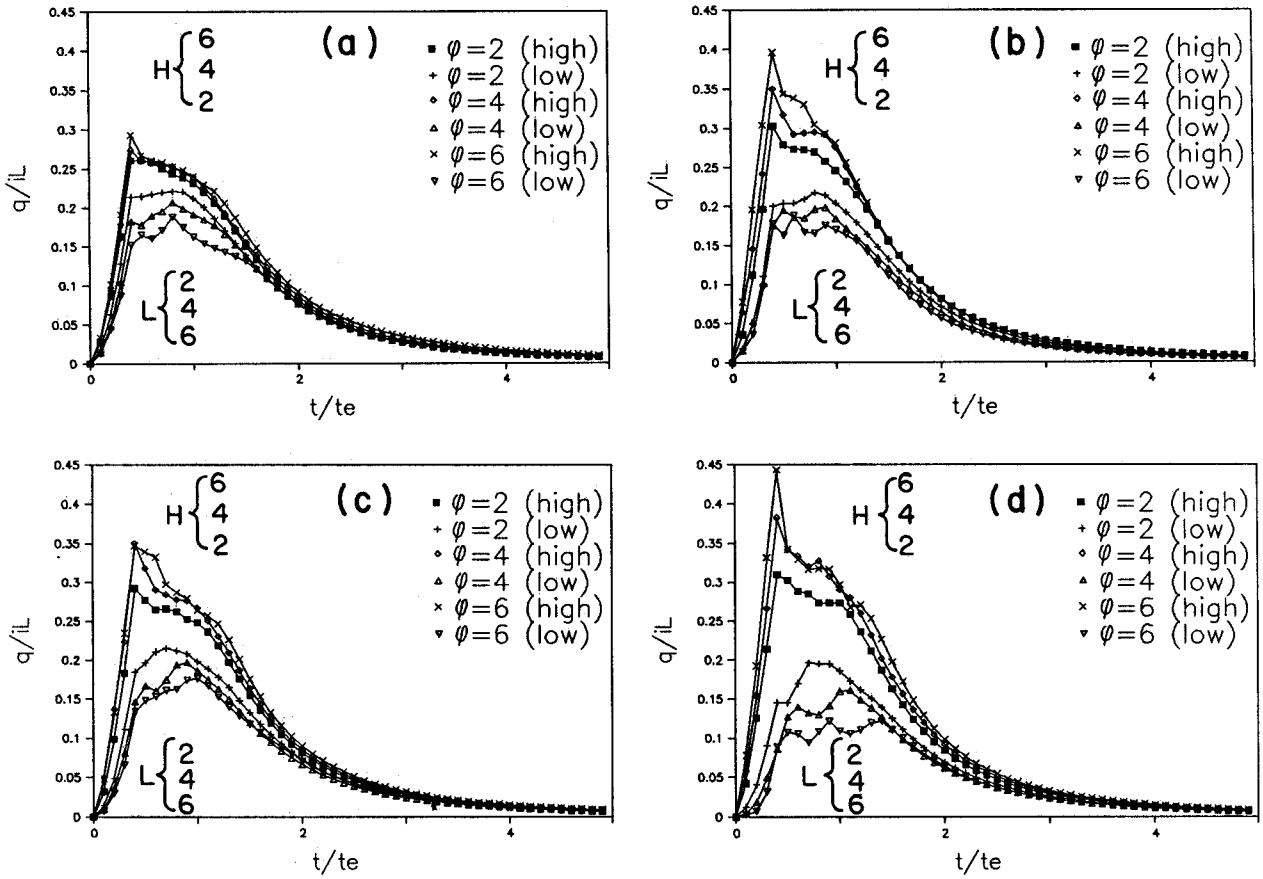

Fig. 5. Hydrograph envelopes for (*a*) slope at $t_r/t_e = 0.4$, (*b*) Manning n at $t_r/t_e = 0.4$, (*c*) surface width at $t_r/t_e = 0.4$, (*d*) rainfall intensity at $t_r/t_e = 0.4$, (*e*) slope at $t_r/t_e = 1.0$, (*f*) Manning n at $t_r/t_e = 1.0$, (*g*) surface width at $t_r/t_e = 1.0$, (*h*) rainfall intensity at $t_r/t_e = 1.0$, (*i*) slope at $t_r/t_e = 5.0$, (*j*) Manning n at $t_r/t_e = 5.0$, (*k*) surface width at $t_r/t_e = 5.0$, and (*l*) rainfall intensity at $t_r/t_e = 5.0$.

hydrographs are selected: $t_r/t_e = 0.4$, 1.0, and 5.0. Simulations are repeated for three different values of ϕ: 2, 4, and 6. The individual effects of the four overland flow parameters are investigated. For each permutation (4 parameters × 3 values of ϕ × 3 values of t_r/t_e), 100 simulations are performed, thus totaling 3600 simulated hydrographs. Given the large amount of data generated from these 3600 hydrographs, the pertinent hydrologic data have been reduced into an interpretable form. First, hydrograph envelopes are considered, followed by deviation hydrographs, relative spatial sensitivity, and finally, distribution of peak discharge.

Hydrograph Envelopes

For each set of 100 equivalent hydrographs a hydrograph envelope is determined from the highest and lowest simulated discharges at each time step. These envelopes, in Figures 5*a*–5*l*, show the maximum variation in discharge as a function of time along the hydrograph. For instance, when $\phi = 2$, all the 100 simulated hydrographs were comprised between the curves $2L$ and $2H$. It is observed that the general shape of these envelopes is primarily a function of the dimensionless ratio t_r/t_e. The degree of variation within a set of hydrographs is quite large for $t_r/t_e = 0.4$, but very small when $t_r/t_e = 5.0$. Interesting results include the following:

1. Figures 5*a*–5*d* show partial equilibrium hydrograph results with the highest simulated discharge occurring at the last time interval experiencing rainfall. The region enclose by the envelopes is much larger than that for $t_r/t_e = 1.0$ c 5.0 (Figures 5*e*–5*l*).

2. When $t_r/t_e = 1.0$ (see Figures 5*e*–5*h*), a particular cas of complete hydrograph is obtained. Notice that these hy drographs exhibit peak discharges near unity at $t/t_e = t_r/t_e$ = 1.0 and then begin to recede. In essence, these hydrograph are like the complete hydrographs without an equilibriu plateau and like the partial hydrographs in that the pea discharge occurs during the last time interval with rainfall

3. When $t_r/t_e \gg 1$ (i.e., $t_r/t_e = 5.0$; see Figures 5*i*–5*l* complete hydrographs are characterized by an equilibriu plateau region where the dimensionless discharge is unit from $t/t_e \approx 1.0$ to $t/t_e = t_r/t_e$. These Figures 5*i*–5*l* demo strate that the numerical model reproduces the expecte results that the dimensionless equilibrium discharge equa unity regardless of the spatial variability of the hydrolog parameters. The runoff variability during the rising an falling limbs can be better analyzed through deviation hy drographs.

Deviation Hydrographs

With reference to Figure 3, the discharge from a nonpe turbed system at any time may be considered as a referenc value about which the discharge from a perturbed syste varies. When considering a set of 100 simulated hydr graphs, the deviation hydrograph measures the standa

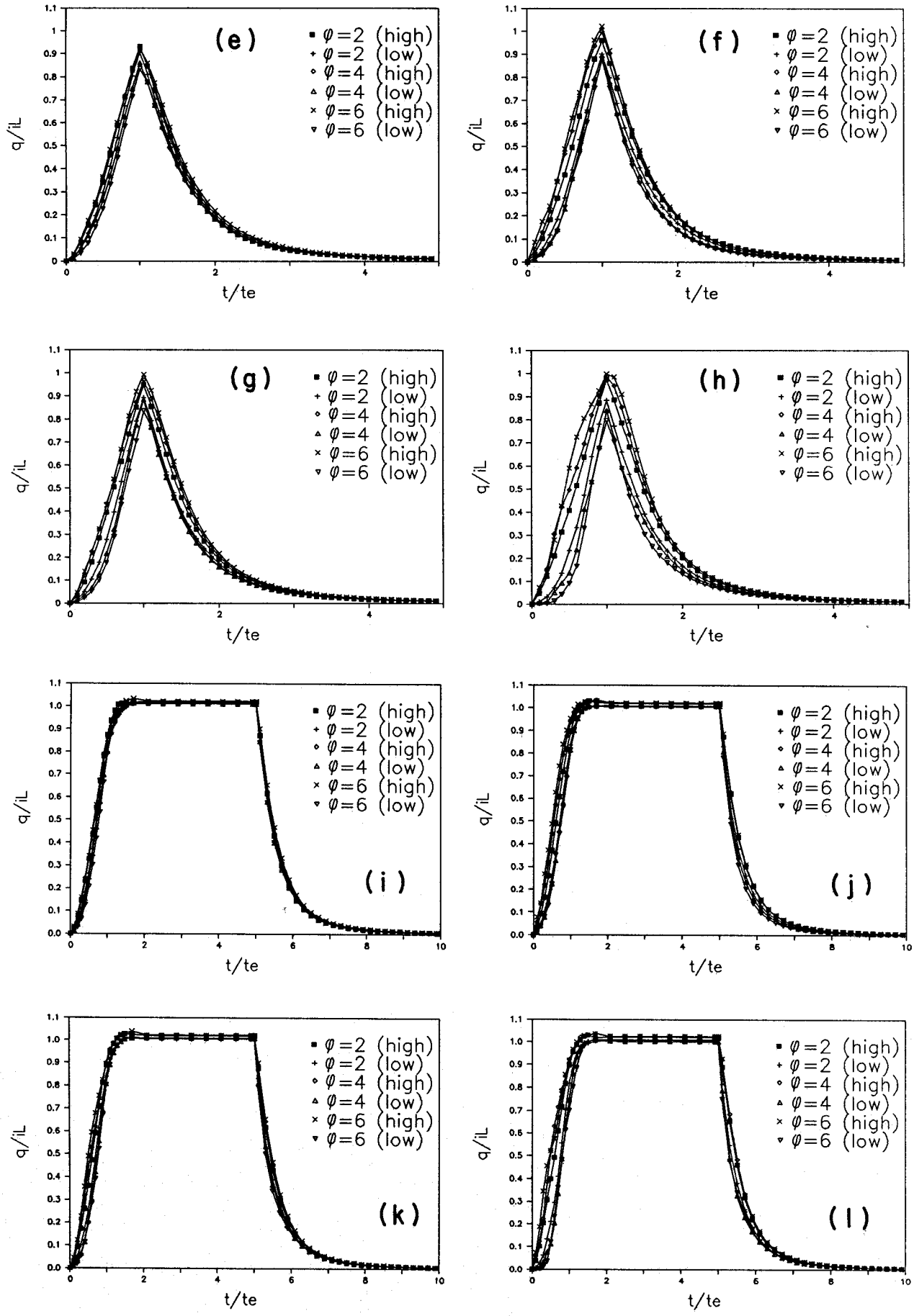

Fig. 5. (continued)

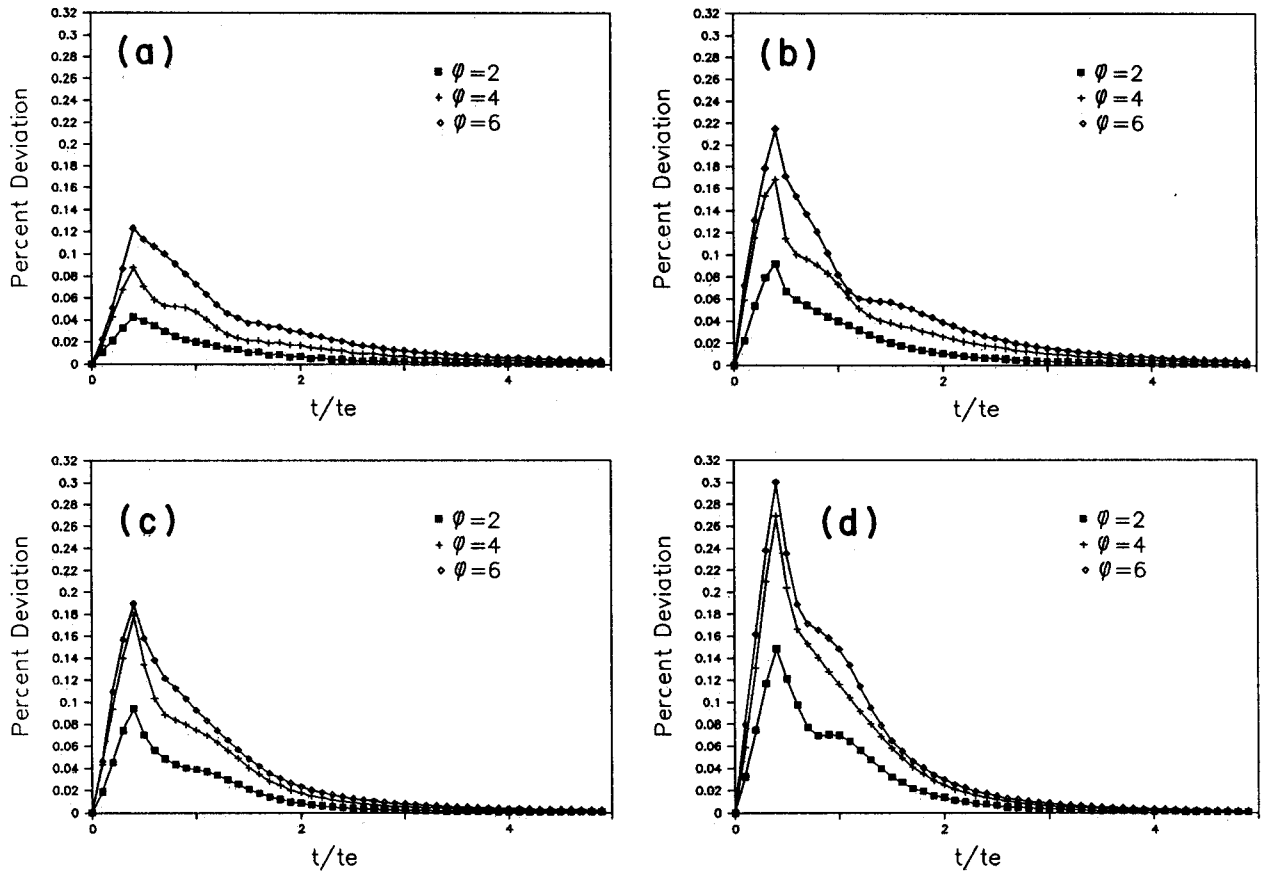

Fig. 6. Deviation hydrographs for (*a*) slope at $t_r/t_e = 0.4$, (*b*) Manning n at $t_r/t_e = 0.4$, (*c*) surface width at $t_r/t_e = 0.4$, (*d*) rainfall intensity at $t_r/t_e = 0.4$, (*e*) slope at $t_r/t_e = 1.0$, (*f*) Manning n at $t_r/t_e = 1.0$, (*g*) surface width at $t_r/t_e = 1.0$, (*h*) rainfall intensity at $t_r/t_e = 1.0$, (*i*) slope at $t_r/t_e = 5.0$, (*j*) Manning n at $t_r/t_e = 5.0$, (*k*) surface width at $t_r/t_e = 5.0$, and (*l*) rainfall intensity at $t_r/t_e = 5.0$.

deviation of the calculated values of discharge about the nonperturbed discharge at each time step:

$$\sigma_t = \sqrt{\frac{1}{m-1}\sum_{k=1}^{m}(q_{k,t} - q_{np,t})^2} \tag{18}$$

where σ_t describes the deviation in output discharge at time t; m is the number of simulated hydrographs (100 in this case); $q_{k,t}$ is the kth perturbed discharge at time t; and $q_{np,t}$ is the nonperturbed discharge at time t. The curve traced out by the deviation hydrograph indicates the magnitude of discharge variation as a function of time.

Dimensionless deviation hydrographs are obtained by dividing the deviation hydrograph σ_t by the partial or complete equilibrium discharge ($\alpha(it_r)^\beta$ when $t_r/t_e < 1.0$; or iL when $t_r/t_e \geq 1.0$). The resulting dimensionless deviation hydrographs in Figures 6*a*–6*l* reflect the percentage variation in discharge relative to the nonperturbed equilibrium discharge. For example, in Figure 6*a* where the slope is spatially varied for a set of 100 equivalent systems, the largest variation in discharge is approximately 0.12 at $t/t_e = 0.4$. This means that the standard deviation of discharges at $t/t_e = 0.4$ is approximately 12% of the peak discharge of the partial equilibrium hydrograph.

Examination of Figures 6*a*–6*l* indicates that the general shape of dimensionless deviation hydrographs is primarily dependent on the value of t_r/t_e regardless of which parameter is spatially varied. The following observations are rather instructive:

1. Figures 6*a*–6*d* exhibit the largest variations in discharge, and therefore the discharge from partial equilibrium systems is highly sensitive to perturbations in any input parameter.

2. The region $t/t_e < 1.0$ in Figures 6*e*–6*l* exhibits a maximum value around $t/t_e = 0.7$. The deviation increases for $t < 0.7t_e$ because the discharges are getting larger. For $0.7t_e < t < t_e$, the deviation decreases with time because the system is approaching equilibrium discharge which, as shown in Figures 5*i*–5*l*, is independent of deviations in the system. Therefore at $t = 0.7t_e$ a balance seems to exist between the opposing trends of near equilibrium behavior and time increasing discharge causing a maximum deviation in discharge. Notice that for $t < 0.4t_e$, the results in Figures 6*a*–6*d* are not directly comparable to those of Figures 6*e*–6*l*. This is because the deviation hydrograph is defined as $\sigma_t/\alpha(it_r)^\beta$ when $t_r < t_e$ and σ_t/iL when $t_r > t_e$.

3. Figures 6*i*–6*l* show the standard deviation in discharge for varying input parameters and $t_r/t_e = 5.0$. Notice again that the maximum deviations in discharge occur at $t/t_e = 0.7$ as was the case for $t_r/t_e = 1.0$. A similar peak is observed for the recession limb, its magnitude in all cases remains smaller than the peak during the rising limb. It can be concluded that spatial variability will primarily affect the rising limb of hydrographs.

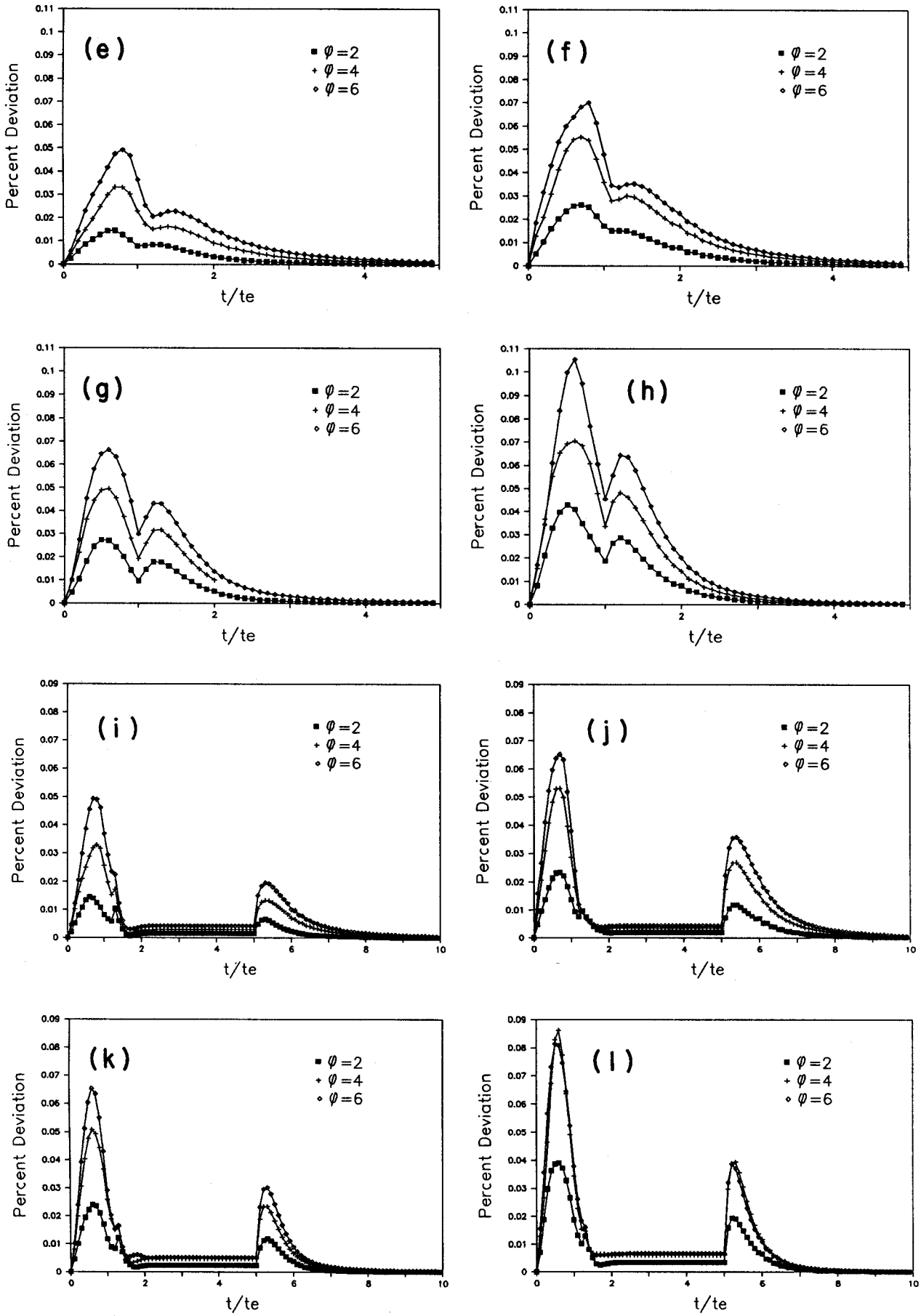

Fig. 6. (continued)

TABLE 1. Relative Spatial Sensitivity $R_{s,l}$

Parameter	ϕ	$t_r/t_e = 0.4$	$t_r/t_e = 1.0$	$t_r/t_e = 5.0$
Slope	2	0.05536	0.03163	0.01005
Slope	4	0.06145	0.03846	0.00948
Slope	6	0.07977	0.04561	0.01161
Manning n	2	0.11648	0.07270	0.02033
Manning n	4	0.11327	0.08260	0.02001
Manning n	6	0.12678	0.08447	0.02048
Surface width	2	0.10987	0.06707	0.01741
Surface width	4	0.11651	0.07523	0.01666
Surface width	6	0.11697	0.07787	0.01860
Rainfall intensity	2	0.19591	0.11301	0.02743
Rainfall intensity	4	0.18717	0.12124	0.02890
Rainfall intensity	6	0.19622	0.12834	0.02522

Relative Spatial Sensitivity

With an understanding of the general behavior of the model response to input variation, the objective of this section is to quantify the spatial sensitivity of the model output to each parameter.

The spatial variability of an input parameter is defined in terms of a coefficient of variation $C_v = \sigma_i/\mu_X$ where σ_i is the standard deviation of the spatially varied input parameter for a set of 100 equivalent systems, and μ_X is the reference value of the same parameter.

The spatial variability of the output discharge is computed with a technique similar in concept to that used by *Wu et al.* [1978]. The hydrograph envelopes presented in Figure 6 can be time-integrated to provide a hydrograph envelope volume ΔV. When divided by the total excess rainfall volume V, the resulting ratio $V^* = \Delta V/V$ describes the spatial variability of the output discharge.

Relative spatial sensitivity $R_{s,t}$ describes the ratio of variation in output per unit variation in input as proposed by *McCuen and Snyder* [1986]:

$$R_{s,l} = \frac{V^*}{C_v} \tag{19}$$

The values of relative spatial sensitivity shown in Table 1 provide a quantitative evaluation of the four input parameters under spatially varied conditions. It is found that excess rainfall intensity shows the highest degree of sensitivity, followed by Manning n, surface width, and finally slope. This is in agreement with the observations of envelope hydrographs in Figure 5 and of deviation hydrographs in Figure 6. This relative spatial sensitivity analysis demonstrates that relative spatial sensitivity values decrease with dimensionless rainstorm duration but remain nearly constant for various ϕ values.

A total of 4800 additional computer simulations (100 runs $\times$ 4 parameters $\times$ 12 values of t_r/t_e = 0.6, 0.8, 1.1, 1.2, 1.3, 1.4, 1.5, 1.6, 1.8, 2.5, 3, 4) were performed to better define the relationship between relative spatial sensitivity $R_{s,t}$ and dimensionless rainstorm duration t_r/t_e in the region of $0.4 \leq t_r/t_e \leq 5.0$. After rescaling the values of $R_{s,l}$ with their reference values at $t_r/t_e = 1.0$, Figure 7 shows the same decrease in sensitivity for each parameter. For example, this general curve shows that the relative spatial sensitivity when $t_r/t_e = 2$ is about 50% of the relative sensitivity when $t_r/t_e = 1$.

Distribution of Peak Discharge

Considering the 100 hydrographs simulated under spatially varied conditions, the values of the peak discharges for each system are ranked and plotted against their nonexceedance probability. Figures 8*a*–8*d* show the distribution of dimensionless peak discharges for several values of t_r/t_e ranging from 0.3 to 2 near the threshold conditions between complete and partial equilibrium hydrographs. These figures clearly illustrate the changes in distribution of peak discharge for perturbed systems when the rainfall duration is approaching time to equilibrium. When $t_r/t_e < 1.0$, peak discharges vary over a wide range of values as indicated by wide-spread distributions in Figures 8*a*–8*d*. As rainfall duration approaches and exceeds the time to equilibrium, the system is forced to peak closer to or at unity as indicated by the steep lines in Figures 8*a*–8*d*.

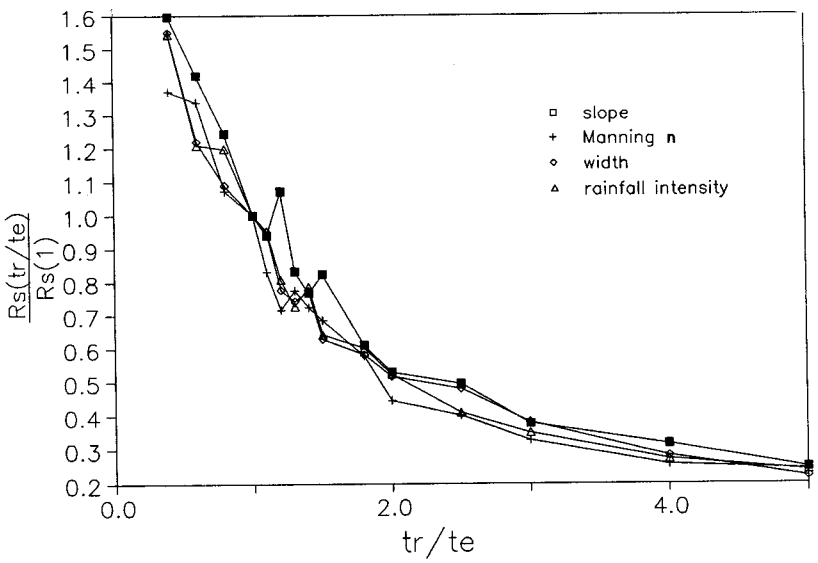

Fig. 7. Relative spatial sensitivity versus dimensionless rainfall duration t_r/t_e.

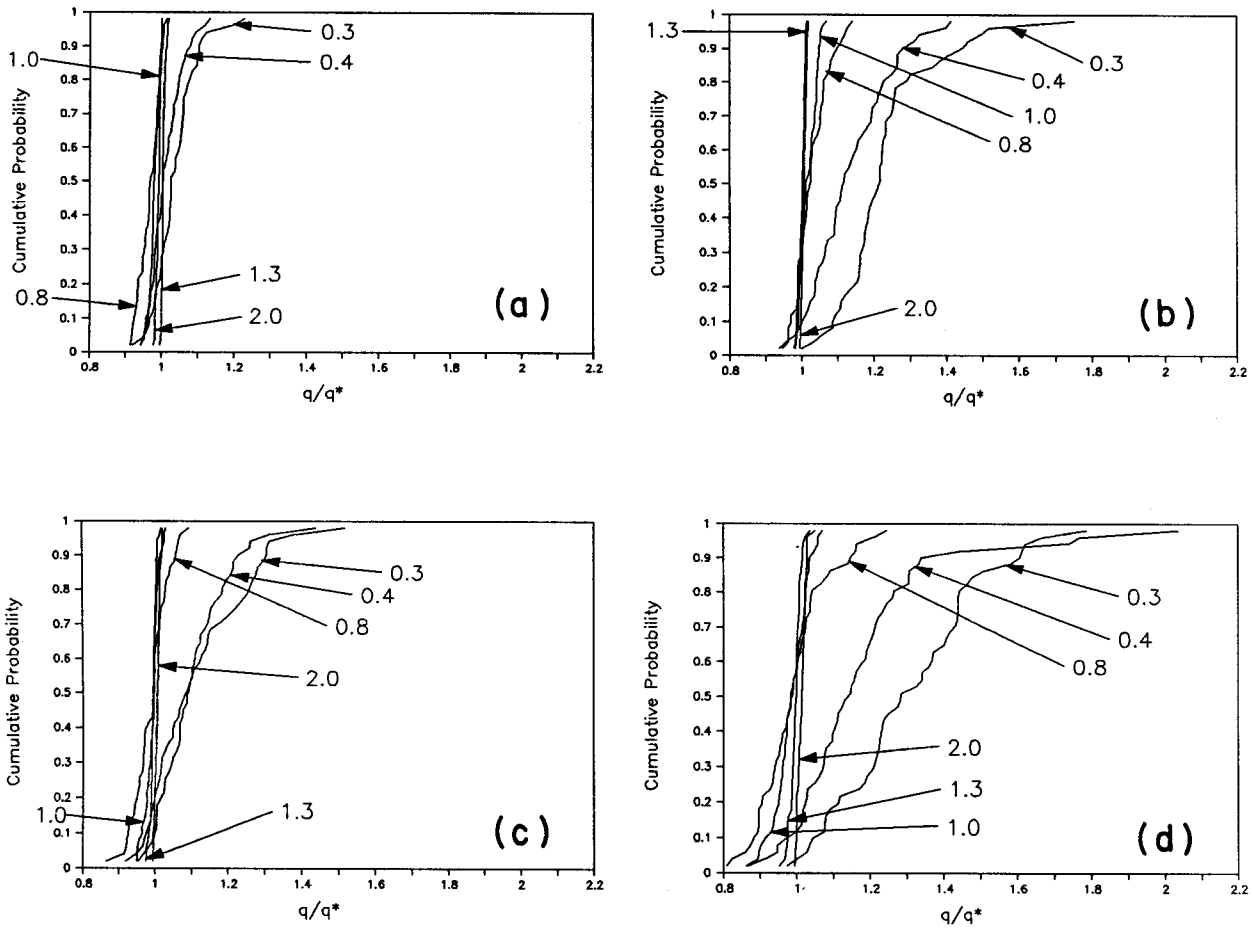

Fig. 8. Distribution of peaks when $0.3 < t_r/t_e < 2$ for (*a*) slope, (*b*) Manning *n*, (*c*) surface width, and (*d*) rainfall intensity.

These figures clearly demonstrate that the distribution of peak discharges changes completely as t_r/t_e approaches unity. For this reason it is concluded that the time to equilibrium under spatially varied conditions remains essentially equal to the time to equilibrium calculated for the nonperturbed system.

Correlated Spatial Variability

The above results for uncorrelated spatially varied hydrologic parameters highlight the primary importance of the time to equilibrium to describe the physical characteristics of a spatially perturbed system. The question of interest in this section regards whether spatial correlation between the perturbed parameters will change the results of the analysis or not. A brief investigation of this problem is presented in this section. The approach taken is based on the reconstitution of surface profiles from spectral density functions of terrain elevation data. Since the results shown in Figure 7 are independent of the parameter selected for the analysis, only surface slope has been selected here, the other parameters being expected to yield similar results.

A terrain height variance spectra is obtained from field measurements of terrain elevations in Steamboat Springs, Colorado. The data sources for this analysis include topographic maps and National Oceanic and Atmospheric Administration/EDIS/NGSDC 30-s average elevation tapes. *Young and Pielke* [1983] converted the data into spectral form using a fast Fourier transform algorithm. Least squares was used to fit the power law relationship:

$$S_z = a\lambda^b \tag{20}$$

where S_z is the terrain height variance in meters squared kilometers, λ is the wavelength of the landform in kilometers, and a and b are the calibrated coefficient and exponent, respectively. For Steamboat Springs, a and b are equal to 2.1 and 0.9, respectively.

The major difference with the random generation scheme described earlier is that spectral data creates spatially correlated slope profiles. By "spatially correlated" it is meant that the slope at one node is somewhat influenced by the slope of adjacent nodes. The result is that the spatially correlated slope profiles have smooth, gradual changes in slope when compared to the rugged randomly generated profiles as shown in Figure 9. Series of 100 spatially correlated slope profiles are generated from (20) for rainfall durations of $t_r/t_e = 0.4$, 1.0, and 5.0. The simulated data are analyzed with the same procedure developed for uncorrelated spatial variability.

A relative sensitivity analysis based on (19) is performed on the spatially correlated profiles for comparison with the spatially uncorrelated profiles. Table 2 shows, again, how R_s decreases as t_r/t_e increases. The absolute values of correlated versus uncorrelated data are meaningless because a larger value of ϕ could have been selected to match the correlated values. Therefore after dividing the values in

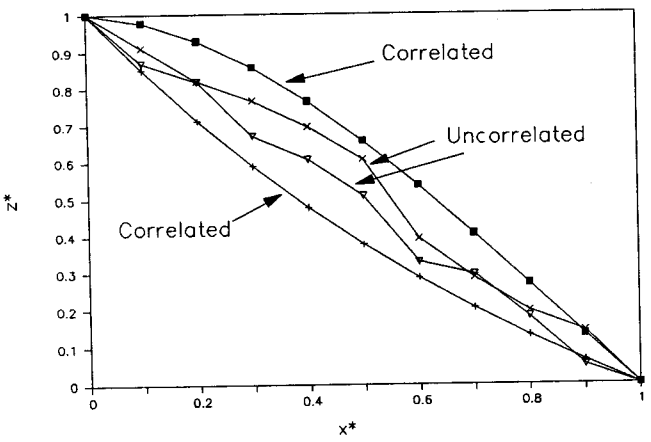

Fig. 9. Comparison of correlated and uncorrelated slope profiles.

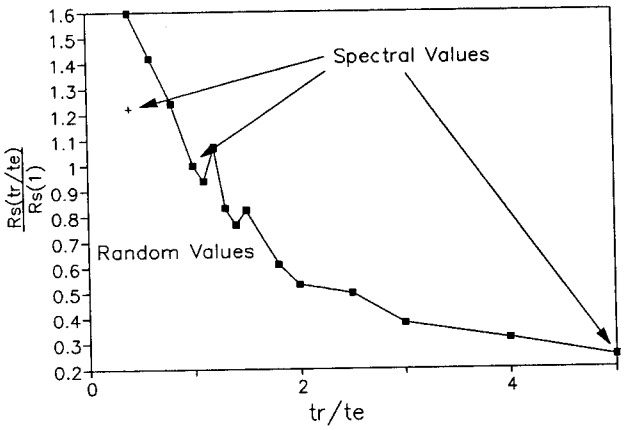

Fig. 10. Relative spatial sensitivity for correlated and uncorrelated ($\phi = 4$) slope profiles.

Table 2 by the relative sensitivity at $t_r/t_e = 1$, the resulting graph in Figure 10 shows the results practically identical to those of Figure 7. From Figure 10 it may be inferred that the decrease of R_s as a function of t_r/t_e is independent of the nature of the slope perturbations.

The primary conclusion is that uncorrelated systems show the same behavior as spatially correlated systems in that the time to equilibrium plays the dominant role in spatially varied surface runoff.

Similarity and Scaling Problems

Similarity conditions for surface runoff generated at different scales can be reassessed considering that spatially varied hydrologic parameters exert little influence on the computed discharge if the duration of rainfall exceeds the time to equilibrium. The criteria used to calculate the time to equilibrium may now be reversed and used to determine the appropriate length scale describing similarity conditions for surface runoff given the rainfall duration t_r, the spatially averaged excess rainfall intensity i, the average slope S, the average surface roughness n, and the average surface width w. The appropriate length scale L_s is then calculated from (5) after considering that $L_s = L$ when $t_r = t_e$:

$$L_s = \frac{\alpha i^{\beta-1}(t_r)^{\beta}}{w} \tag{21}$$

or, specifically for Manning equation,

$$L_s = \left[\frac{t_r^{5/3} S_0^{1/2} i^{2/3}}{n}\right] \tag{22}$$

where the length scale L_s is in meters, the rainfall duration t_r is in seconds, and the rainfall intensity i is in meters per second. Notice that the length scale does not depend solely on the configuration of the catchment but also depends on the characteristics of the storm to be investigated. Indeed, both the rainfall duration t_r and the spatially averaged excess rainfall intensity i are needed for the determination of the length scale. Under these conditions the length scale L_s means that the spatial variability at a field runoff length smaller than L_s has a negligible influence on the computed discharge. At this scale the runoff response to rainfall input also becomes nearly linear as $t_r/t_e \to \infty$. Conversely, field runoff lengths in excess of the length scale produce a nonlinear rainfall-runoff relationship which is highly sensitive to spatial variability of the hydrologic parameters.

The following practical example determines if the spatial variability in topography and surface roughness will largely influence calculations of surface runoff. The spatially averaged values are given for the slope $S_0 = 0.03$, runoff length $L = 500$ m, Manning $n = 0.02$, rainfall duration $t_r = 3600$ s (1 hour) and excess rainfall intensity $i = 7.06 \times 10^{-6}$ m/s (1 inch per hour). The length scale calculated from (22) exceeds the runoff length ($L_s = 2690$ m $> L = 500$ m) which indicates that the spatial variability in topography and surface roughness exerts little influence on the calculations of surface runoff from spatially averaged values of the hydrologic parameters. For this rainstorm the spatial variability effects would be important at runoff lengths $L > L_s = 2690$ m.

TABLE 2. Relative Spatial Sensitivity for Correlated and Uncorrelated ($\phi = 6$) Slope Profiles

Distribution	$t_r/t_e = 0.4$	$t_r/t_e = 1.0$	$t_r/t_e = 5.0$
Correlated	0.2046	0.1672	0.0432
Uncorrelated ($\phi = 6$)	0.0798	0.0456	0.0116

Conclusions

This study quantifies the influence of spatial variability in slope, surface roughness, surface width, and excess rainfall intensity on surface runoff characteristics. Comparisons of similar one-dimensional systems involve finite element surface runoff simulations for stationary rainstorms using the kinematic wave approximation of the St-Venant equations combined with Manning's resistance formula. Similarities between all input parameters are strictly preserved by keeping identical spatially averaged values of all input parameters for each run. Also, the same excess rainfall volume is maintained in all runs in order to avoid the error and bias problems discussed in the recent literature. The results of both correlated and uncorrelated spatial variability are expressed in dimensionless form after considering that the time to equilibrium serves as an important physical characteristic. These similarities in rainfall-runoff response under spatially varied hydrologic conditions serve to define a length scale describing similar sensitivity to spatially varied surface runoff conditions.

This investigation demonstrates that the finite element method is an extremely powerful tool for fundamental hydrologic investigations on overland flow generated under spatially varied conditions. Not only does the finite element method provide efficient solutions (8400 computer simulations are summarized in this paper) to the kinematic wave approximation of the governing surface runoff equations, but it permits quantitative evaluations of the effects of spatial variability in terms of physically based dimensionless parameters such as dimensionless discharge q/iL, dimensionless time t/t_e, and dimensionless rainfall duration t_r/t_e.

The primary conclusions reached from this investigation can be listed as follows:

1. A length scale describing similarity in surface runoff generated under spatially varied hydrologic conditions is defined as a function of both the surface parameters and the duration and excess rainfall intensity of rainstorms.

2. For field runoff lengths much shorter than the length scale, the spatial variability exerts little influence on the runoff hydrograph, and the rainfall-runoff relationship becomes nearly linear. Conversely, at field runoff lengths exceeding the scale length, the spatial variability causes variations in calculated runoff discharges and the rainfall-runoff relationship becomes nonlinear.

3. The time to equilibrium of spatially varied systems remains essentially equal to the time to equilibrium calculated from spatially averaged values of hydrologic parameters.

4. The results of the relative spatial sensitivity in Figure 7 are identical for each of the four parameters considered.

5. The results of relative spatial sensitivity in Figure 10 are remarkably similar for both correlated and uncorrelated spatial variability.

6. The deviation hydrographs in Figure 6 show that the maximum variability in runoff discharge occurs during the rising limb of the hydrograph.

7. The distribution of peak discharges in Figure 8 changes drastically as the dimensionless rainfall duration approaches unity.

The length scale can serve as a basis for the determination of grid size in hydrologic models. Extreme events with large rainfall durations and intensity can be analyzed with coarser grids than most common rainstorms.

Acknowledgments. This study has been completed by the Hydrologic Modeling Group of the Center for Geosciences at Colorado State University. The financial support granted by the U.S. Army Research Office (grant ARO/DAAL 03-86-K-0175) is gratefully acknowledged. We are thankful to R. Pielke from the Department of Atmospheric Sciences at Colorado State University who provided the spectral data and expertise needed for the correlated spatial variability analysis.

REFERENCES

Amorocho, J., Stochastic modeling of precipitation in space and time, in *Statistical Analysis of Rainfall and Runoff*, pp. 3–20, Water Resources Publications, Littleton, Colo., 1982.

Amorocho, J., and B. Wu, Mathematical models for the simulation of cyclonic storm sequences and precipitation fields, *J. Hydrol.*, *32*, 329–345, 1977.

Caroni, E., R. Rosso, and F. Siccardi, Nonlinearity and time-variance of the hydrologic response of a small mountain creek, in *Scale Problems in Hydrology*, pp. 19–37, D. Reidel, Hingham, Mass., 1986.

Dawdy, D. R., A review of deterministic surface water routing in rainfall-runoff models, in *Rainfall-Runoff Relationships*, pp. 23–36, Water Resources Publications, Littleton, Colo., 1982.

Dhatt, G., and G. Touzot, *The Finite Element Method Displayed*, John Wiley, New York, 1984.

Diaz-Granados, M., R. L. Bras, and J. B. Valdes, Incorporation of channel losses in the geomorphologic IUH, in *Scale Problems in Hydrology*, pp. 217–243, D. Reidel, Hingham, Mass., 1986.

Eagleson, P. S., *Dynamic Hydrology*, McGraw-Hill, New York, 1970.

Gupta, V. K., and E. C. Waymire, A stochastic kinematic study of subsynoptic space-time rainfall, *Water Resour. Res.*, *15*(3), 637–644, 1979.

Henderson, F. M., and R. A. Wooding, Overland and groundwater flow from a steady rainfall of finite duration, *J. Geophys. Res.*, *69*(8), 1531–1540, 1964.

Julien, P. Y., and D. B. Simons, Sediment transport capacity of overland flow, *Trans. ASAE*, *28*(3), 755–762, 1985.

Julien, P. Y., G. E. Moglen, and G. U. Sunada, CASC user's manual—A finite element model for spatially varied overland flow simulation, *Rep. CER 87-88 GEO7*, Colo. State Univ., Fort Collins, 1988.

Kibler, D. F., and D. A. Woolhiser, The kinematic cascade as a hydrologic model, *Hydrol. Pap. 39*, Colo. State Univ., Fort Collins, 1970.

Lighthill, M. H., and G. B. Whitham, On kinematic waves, I, Flood movement in long rivers, *Proc. R. Soc. London, Ser. A*, *229*, 281–316, 1955.

Machado, D., and T. O'Donnell, A stochastic interpretation of a lumped overland flow model, in *Proceedings of the Fort Collins Third International Hydrological Symposium on Theoretical and Applied Hydrology*, pp. 259–269, Water Resources Publications, Fort Collins, Colo., 1977.

Maller, R. A., and M. L. Sharma, An analysis of areal infiltration considering spatial variability, *J. Hydrol.*, *52*, 25–37, 1981.

McCuen, R. H., and W. M. Snyder, *Hydrologic Modeling—Statistical Methods and Applications*, Prentice-Hall, Englewood Cliffs, N. J., 1986.

Milly, P. C. D., and P. S. Eagleson, Effects of spatial variability on annual average water balance, *Water Resour. Res.*, *23*(11), 2135–2143, 1987.

Moglen, G. E., The effects of spatial variability of overland flow parameters on runoff hydrographs, M.S. thesis, Civ. Eng. Dep., Colo. State Univ., Fort Collins, 1989.

Overton, D. E., and M. E. Meadows, *Stormwater Modeling*, Academic, San Diego, Calif., 1976.

Richardson, J. R., The influence of moving precipitation fields on rainfall-runoff processes, Ph.D. dissertation, Dep. of Civ. Eng., Colo. State Univ., Fort Collins, 1989.

Rodriguez-Iturbe, I., and P. S. Eagleson, Mathematical models of rainstorm events in space and time, *Water Resour. Res.*, *23*(1), 181–190, 1987.

Sharma, M. L., R. J. W. Barron, and E. S. De Boer, Spatial structure and variability of infiltration parameters, in *Advances in Infiltration*, pp. 113–121, American Society of Agricultural Engineers, St. Joseph, Mich., 1983.

Sivapalan, M., and E. F. Wood, Spatial heterogeneity and scale in the infiltration response of catchments, in *Scale Problems in Hydrology*, pp. 81–106, D. Reidel, Hingham, Mass., 1986.

Sivapalan, M., K. Beven, and E. F. Wood, On hydrologic similarity, 2,A scaled model of storm runoff production, *Water Resour. Res.*, *23*(12), 2266–2278, 1987.

Smith, R. E., and R. H. B. Hebbert, A Monte Carlo analysis of the hydrologic effects of spatial variability of infiltration, *Water Resour. Res.*, *15*(2), 419–429, 1979.

Troutman, B. M., Runoff prediction errors and bias in parameter estimation induced by spatial variability of precipitation, *Water Resour. Res.*, *19*(3), 791–810, 1983.

Troutman, B. M., Errors and parameter estimation in precipitation-runoff modeling, 1, Theory, *Water Resour. Res.*, *21*(8), 1195–1213, 1985*a*.

Troutman, B. M., Errors and parameter estimation in precipitation-runoff modeling, 2, Case study, *Water Resour. Res.*, *21*(8), 1214–1222, 1985*b*.

Valdes, J. B., I. Rodriguez-Iturbe, and V. K. Gupta, Approximations of temporal rainfall from a multidimensional model, *Water Resour. Res.*, *21*(8), 1259–1270, 1985.

Wilson, C. B., J. B. Valdes, and I. Rodriguez-Iturbe, On the influence of the spatial distribution of rainfall on storm runoff, *Water Resour. Res.*, *15*(2), 321–328, 1979.

Wood, E. F., M. Sivapalan, K. Beven, and L. Band, Effects of spatial variability and scale with implications to hydrologic modeling, *J. Hydrol.*, *102*, 29–47, 1988.

Woolhiser, D. A., and J. A. Liggett, Unsteady, one-dimensional flow over a plane: The rising hydrograph, *Water Resour. Res.*, *3*(3), 753–771, 1967.

Woolhiser, D. A., and H. B. Osborn, A stochastic model of dimensionless thunderstorm rainfall, *Water Resour. Res.*, *21*(4), 511–522, 1985.

Wu, Y. H., V. Yevjevich, and D. A. Woolhiser, Effects of surface roughness and its spatial distribution on runoff hydrographs, *Hydrol. Pap. 96*, Colo. State Univ., Fort Collins, 1978.

Young, G. S., and R. A. Pielke, Application of terrain height variance spectra to mesoscale modeling, *J. Atmos. Sci.*, *40*(10), 2555–2560, 1983.

P. Y. Julien and G. E. Moglen, Department of Civil Engineering, Engineering Research Center, Colorado State University, Fort Collins, CO 80523.

(Received October 6, 1989;
revised January 30, 1990;
accepted February 20, 1990.)